RESEARCH ARTICLE

Multiple pinhole nuclear imaging using targeted nano-particles for accurate tumors margin detection

A Schwarz, A Shemer, Y Danan

Schwarz A, Shemer A, Danan Y. Multiple pinhole nuclear imaging using targeted nano-particles for accurate tumors margin detection. 2022;6(4):1-7.

Abstract

In order to achieve accurate tumors margin detection, nano-particles are being used for more detailed nuclear imaging. The resolution of nuclear imaging systems is very limited and therefore, magnification is needed. For magnified imaging, a single pinhole collimator (typically a double cone shape), between the object and the gamma detector, can collect magnified projections. The sensitivity in gamma imaging systems such as SPECT using a pinhole collimator, is inversely proportional to the square of the object to pinhole distance. However, the projection size on the gamma detector (which is relative to the size of the object) is determined by the ratio of the distance between detector to pinhole and the distance between pinhole to object. The sensitivity of the pinhole SPECT system must increase severely for using nano-particles in nuclear imaging. Thus, a multiple pinhole SPECT is used. A novel configuration utilizes improved sensitivity efficiency with no resolution reduction for nano-particles objects imaging. The gamma imaging system is based on time multiplexing super resolution method using variable and dynamic pinhole arrays.

Key words: *Nano-particles; Phytochemicals; Organic preservative; Refined palm kernel oil; Storage stability*

INTRODUCTION

One of the main problems in cancer resection surgeries is the recurrence of the disease after tumor resection surgery [1,2]. In order to prevent a local recurrence of the disease and a reoperation procedure, a complete excision is critical. Currently, following the surgical procedure, routine histological tests are usually done for tumor margins examinations [3]. Through the past few years, a few intraoperative tumor margin detection methods have been developed with some success. However, a highly sensitive and specific intraoperative tumor margin detection technique is still required that will decrease the recurrence of the cancer and the need of repeated medial operation [4,5]. This high sensitivity detection is much more crucial when the cancerous tissue growth nearby neurological systems, and it is hazardous to resect an extra tissue [6,7].

Several techniques have been developed over the years in order to achieve better tumor margins visualization, such as: CT, MRI and fluorescence imaging. However, those methods have limited resolution derived from tissue displacement during operation, and other problems [8,9].

Numerous research groups have used Gold Nanoparticles (GNPs) biomarkers as imaging contrast agents and also for other biomedical applications such as drug delivery and therapeutics. These nano-particles are specifically targeted to attach the surface of cancer cells (Figure 1).

Therefore, accurate tumors margin detection is needed [10,11]. One of the main methods for functional imaging used today is nuclear imaging. Two major techniques are used in the field of human clinical radionuclide imaging: Single Photon Emission Computed Tomography (SPECT) and Positron Emission Tomography (PET). These techniques are especially important for fields such as: Highly sensitive molecular imaging in the study of human diseases, the testing of new pharmaceuticals, the development of new tracers for imaging and the understanding of biological mechanisms [12,13].

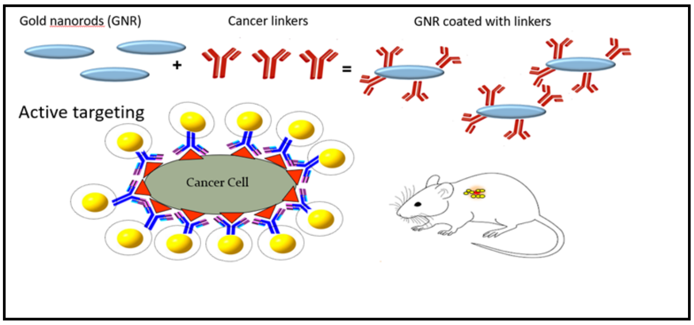

Figure 1) *The active targeting using nano-particles attach to the surface of cancer cells*

The use of a collimator in SPECT systems is due to the disadvantage of a gamma camera, in that despite its ability to absorb gamma photon emission, it cannot provide information on the direction from which it was emitted [14,15]. A parallel hole collimator made of lead is placed in front of the gamma camera and allows photons at only zero-degree angle to reach the gamma detector. The disadvantage of using a collimator is in blocking many photons and thus severely impairing the efficiency of detection [16,17]. Another disadvantage of this technique is in obtaining an unmagnified imaging system where the image size depends directly on the size of the detector. Since lenses are not used in the gamma system, in order to obtain magnification, the collimator is replaced with a pinhole [18,19]. Unlike a collimator, the pinhole replaces a lens and provides the information about the direction from which the photon is emitted. In this way the gamma detector can absorb photons from different angles and not just zero-degree angled photons as well as provide magnification capability in the imaging system. The magnification is determined by the ratio of the distances between the pinhole to the detector and the object to the pinhole [20,21]. Using a M-magnification system is equivalent to using a detector with a M-resolution better. The imaging system characteristics determined by the shape, size and material of the pinhole. The main disadvantage of the pinhole is the aperture size that limits the number of photons that can eventually reach the detector [22,23].

Department of Electrical Engineering, Azrieli Jerusalem College of Engineering, Schreiboim, Jerusalem, Israel

Correspondence: Shemer A, Electrical Engineering, Azrieli Jerusalem College of Engineering, Schreiboim, Jerusalem, Israel, E-mail: arielsc@jce.ac.il

Received: October 29, 2019, Manuscript No. PULJNN-19-3986; Editor assigned: November 01, 2019, PreQC No. PULJNN-19-3986 (PQ); Reviewed: November 15, 2019, QC No. PULJNN-19-3986; Revised: July 22, 2022, Manuscript No. PULJNN-19-3986 (R); Published: August 19, 2022, DOI: 10.37532/1308-4038.6.4 1-7.

MATERIALS AND METHODS

In order to solve this problem and increase the sensitivity of the system, a multi-pinhole array can be used. Such an array structure increases the aperture of the imaging system and thus allows simultaneous capture of the gamma projection and increase the number of photons [24,25]. This multi-pinhole structure can also be used to obtain a 3D imaging with only one gamma detector. There are several methods to get a 3D gamma imaging system. One method for gamma systems uses a dynamic structure in which an array of detectors rotates relative to the object but thereby increases the scanning time when in terms of convenience, it is most common to rotate the detectors array while the object is stationary [26,27]. Another method of obtaining 3D gamma imaging is by using a stationary multi-pinhole array with simultaneous capture. This stationary structure is suited for dynamic scans with short scan time. When using a multiple pinholes array there are duplicates of the object on the gamma detector that can cause overlapping problems. Reconstruction algorithms (analytic or iterative) are used, such as the iterative method of Ordered Subsets Expectation Maximization (OSEM), to reconstruct the image from overlapped projections in a multiplexed multi-pinhole SPECT system [28,29]. There are number of considerations for designing a multi-pinhole array that affect the features of the gamma imaging system such as: The size and number of the pinholes, the acceptance angle, the distances of the system components (magnification) and the overlapping degree (multiplexing of the pinhole projections on the detector). Focusing all pinholes to a small volume of interest can achieve sensitivity improvements as obtained in focused multi-pinhole gamma systems [30,31].

RESULTS AND DISCUSSION

In the field of nuclear medicine, the first system with a multi-pinhole array was presented by Vogel. The multi-pinhole array was consisting of seven pinhole the transferred seven non-overlapping projections on the gamma detector [32,33]. This array structure was designed to achieve 3D imaging rather than to improve sensitivity of the 2D image. A similar system with an optimized multi-pinhole array was presented by Ivanovic, acquiring a nonmultiplexed projections over a limited angular range. Others stationary SPECT systems with no overlapping projections have been suggested based on a larger number of single pinhole detectors [34,35]. SPECT systems that perform gamma imaging from multiplexed projection data (overlapping pinhole projections), were introduced by Meikle and Wilson, consisting of one or more multi-pinhole detectors rotating around the object. Another method using a synthetic aperture was introduced by Wilson. The synthetic aperture data was collected from one direction but for different distances of pinhole to detector [36,37]. Other multi-pinhole designs for SPECT system have been suggested, with various of properties. Another approach to the overlapping problems is the usage of Coded Aperture Imaging (CAI). Mertz and Young were the first to introduce a coded aperture system for imaging X-ray stars, using an off-axis Fresnel zone plate. The decoding process was done by using coherent light. Appling to nuclear medical imaging, Barrett et al. used this method for planar 2D imaging and limited 3D imaging of small objects [38,39]. There system consisted of a grid of lead, placed in front of the object to reduce the background associated with CAI and to enable continuous imaging of the gamma-ray sources performed by the off axis zone plate [40,41]. For the X-ray astronomy field, Dicke suggested number of random pinholes, with an average transmission of 50% as a design of CAI. Over the years, many other have tried to suggest improvements to the X-ray and gamma ray imaging systems [42,43]. Accorsi adapted the CAI technique to near field geometry of medical imaging. The common problem for all those suggested multi-pinhole and coded aperture designs is the narrow Optical Transfer Function (OTF) that causes loss of information. Both the OTF of a single pinhole and the OTF of multi-pinhole array causes loss of information due to the zero points in the OTF that affect the final reconstruction [44,45].

The imaging concept

In order to obtain the advantages of multi-pinhole and coded aperture arrays on one hand, that provides improved resolution through magnification as well as high sensitivity (due to the large number of pinholes) and on the other hand to avoid the loss of information due the OTF's zero points that affect the reconstruction image, we propose a novel approach [46,47]. Based on our previous work, presenting a lensless imaging concept of a multi Variable Coded Aperture (VCA) design for far field and near field imaging, we apply this new approach to gamma radiation imaging applications. In this research we present coded aperture design with variable multi pinhole array and time multiplexing for gamma imaging applications [48,49]. By using variable array with time multiplexing approach although each static array of time interval has zero points in its OTF, the overall variable array maintains higher spatial frequencies of the object. The design of a time variated multi-pinhole array instead of a static multi-pinhole is essential to avoid the loss of information. A time multiplexed variable multi pinhole array creates the complement encoding aperture with minimum loss of information in compare to the static multi-pinhole array with the same number of pinholes [50]. Simplicity and flexibility are the main advantages of such a system and allow a wide range of array design options. The array design parameters determine the characteristics of the gamma imaging system such as the sensitivity efficiency improvement factor and the Signal to Noise Ratio (SNR). While preserving the same image quality, the proposed design shortens the scan time. Additionally, since the system allows magnification it enables usage for human clinical radionuclide imaging as well as for biological research with small-animal objects imaging. The concept is modular and allows its integration into an existing gamma system to improve its performance[51-53].

The time multiplexed captured image is reconstructed to the final image. The final image is obtained after properly processing the captured image during the multi pinhole array variation. The time multiplexing image is equivalent to the sum of a set of L captured images. The variable states of the multi-pinhole array are composed of L static pinholes arrays (array for each time interval). Each time state array designed differently and have different parameters such as spacing d (the pitch of the holes in the array). The distances between the pinholes in the same array time state are not necessarily equal. While changing the pinholes distances in each time interval of the coding part, the distance between the planes (U,V) that determines the magnification remain constant. The size of the pinholes (δ) can be constant or can be changed according to the parameters design[54].

We examine the case of a single pinhole to understand the operation principle of the proposed configuration. The pinhole is acting as lens and the imaging is obtained in contrast to the array of channels[55-58].

The magnification ratio of the imaging system is:

$$M = \frac{V}{U} \qquad (1)$$

In the case of an array of multi-pinholes the same operation principle is obtained. However, this time the image obtained at the image plane consists of overlapped image replications of the inspected object from each pinhole. Let examine a simple case of odd number of pinholes with central pinhole and equal distances between pinholes[59-64].

The distances between replications are proportional to the pitch d between the pinholes in the multi-pinhole array. Thus, the captured image obtained is:

$$s_R(x) = \sum_{n=-\frac{N-1}{2}}^{\frac{N-1}{2}} s(x+nd) \qquad (2)$$

Where N is the number of pinholes and s(x) is the image captured with a single pinhole. The result is spatially low passed (with reduced spatial resolution). This can be seen by computing the spectrum of the spatial distribution of Eq. 2:

$$S_R(\mu) = \int s_R(x) e^{-2\pi i x \mu} dx = S(\mu) \cdot F(\mu) \qquad (3)$$

Where S(μ) and F(μ) are the Fourier transforms as follow:

$$S(\mu) = \int s(x) e^{-2\pi i x \mu} dx$$
$$F(\mu) = \sum_{n=-\frac{N-1}{2}}^{\frac{N-1}{2}} e^{-2\pi i n d \mu} \qquad (4)$$

Therefore, F (μ) is basically a low pass filter that cuts off the high spatial frequencies of the imaged object. The cut off frequency is roughly proportional to:

$$\mu_{cutoff} = \frac{1}{Nd} \qquad (5)$$

The smallest spatial feature in the imaging system is proportional to Nd (image plane) or Nd/M (object plane). Increasing the number of pinholes in the array will increase the sensitivity efficiency factor proportionally for 2D array design. The resolution of s (x) is limited by the pinhole size. However, the overall resolution is reduced to the limit described by Eq. 5 due to the summation[60-64]. From optics point of view (regardless to the detector resolution), we denote the wavelength, the size of the pinhole and the size of the smallest feature in the image plane. The following resolution limitation is obtained by:

$$\rho = \frac{\lambda V}{\delta} \qquad (6)$$

The variable imaging system capture L images while changing the pinholes array between each capture while trying to recover the original resolution of Eq. 6 by applying matrix inversion. This is our applied super resolved algorithm.

By changing the pitch d of the holes in the pinholes array in each time interval we get different filters as we can see in the next equations:

$$\begin{aligned} S_R^{(1)}(\mu) &= S(\mu) \cdot F^{(1)}(\mu) \\ S_R^{(2)}(\mu) &= S(\mu) \cdot F^{(2)}(\mu) \\ &\vdots \\ S_R^{(L)}(\mu) &= S(\mu) \cdot F^{(L)}(\mu) \end{aligned} \qquad (7)$$

and in general:

$$S_R^{(l)}(\mu) = S(\mu) \cdot F^{(l)}(\mu) \qquad (8)$$

Where SR (l) (μ) is the Fourier transform of the L set of images:

$$S_R^{(l)}(\mu) = \int s_R^{(l)}(x) e^{-2\pi i x \mu} dx \qquad (9)$$

Each filter causes a loss of information due to each array OTF and this will damage the reconstruction. In the following example one can see the areas in the filter (frequency domain) where there will be zero points with loss of information. For N=3 and equal d we get:

$$\begin{aligned} & s_R(x) = s(x-d) + s(x) + s(x+d) \\ & S_R(\mu) = \int s(x) e^{-2\pi i x \mu} dx = \\ & S(\mu)[e^{-i2\pi\mu d} + 1 + e^{i2\pi\mu d}] = S(\mu) \cdot F(\mu) \\ & F(\mu) = [e^{-i2\pi\mu d} + 1 + e^{i2\pi\mu d}] \end{aligned} \qquad (10)$$

Where sR is the obtained spatial and SR is the obtained spectral distributions.

Here we can see areas (zero points) in frequency domain where some of the object information lost and cannot be reconstructed (Figure 2). P.T.F. stands for Pinhole Transfer Function and it represents a relative unit that is normalized to the transfer function of a single pinhole and equal to 1 (100%) for a single pinhole.

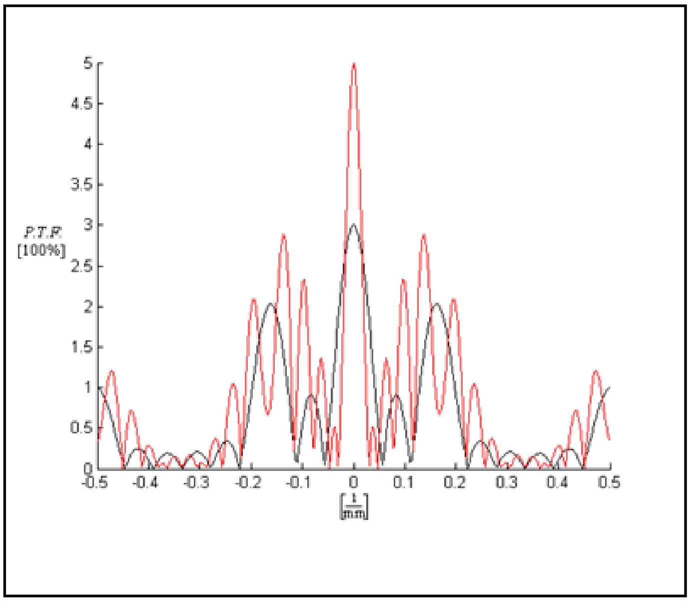

Figure 2) *The F (μ) filter: FFT of the LPF and the spectral areas with loss of information due to zero points in the spectral area. The pinholes array filter with N=3 (black) and with N=5 (red)*

In order minimize the loss of information we need to preserve all the spatial frequencies of the original object image. We control three free parameters in our configuration design: The spatial position of the pinholes in each array state, the number of pinholes in each array state and the capture time interval for each pinhole array state. We choose the parameters such that there will be no information and frequency loss in the filters' sum G (μ):

$$\sum_{l=1}^{L} S_R^{(l)}(\mu) = S(\mu) \cdot \sum_{l=1}^{L} F^{(l)}(\mu)$$
$$G(\mu) = \sum_{l=1}^{L} F^{(l)}(\mu) \qquad (11)$$

We denote by sR (l) (x) as the l image out of the L images summed at the detector to the captured image. In the next examples the time intervals are equal although it is not obligatory and can controlled to control the energy level contributed by each array state in the set to the overall sum G (μ).

The original image s(x) is extracted from the set of images sR (l) (x) by using the inverse of the filters sum G(μ) with better sensitivity efficiency and

SNR. The reconstruction algorithm is performed in the spatial plane (Fourier):

$$S(\mu)=\left[\sum_{l=1}^{L} S_R^{(l)}(\mu)\right]\cdot G(\mu)^{-1} \qquad (12)$$

Hence, the sensitivity efficiency improvement factor is:

$$\eta=\frac{N}{L}\cdot\frac{\pi R_{array}^2}{\pi R_{one}^2}=\frac{N}{L}\cdot\frac{\delta_{array}^2}{\delta_{one}^2} \qquad (13)$$

The first term in the equation is the ratio between total the number of pinholes in the array states (N) and number of array states (L). Note, that L is related to time axis.

The second term in the equation is the ratio between the area of the pinhole in the array system and the area of the pinhole in the single pinhole system. Reducing the value of δ array improves resolution while affecting the radiation activity. In multi-pinhole array systems aiming to improve sensitivity efficiency regardless to resolution, the pinholes size can be equals to single pinhole system (the second term equals 1).

The resolution improvement of the multi-pinhole array system when compared to M=1 system is proportional to the magnification M. Notice that the inverse filter has some disadvantages of noise amplification and thus other filters and algorithms can be used in the system reconstruction, according to the proper application, for example matched filter, Wiener filter, Tikhonov regularization, Richardson-Lucy algorithm and more.

The multi-pinhole arrays design

An array design in one dimension were simulated to investigate the parameters of the variable mutli-pinhole array system. The time multiplex configuration consisted of three array states for three time intervals of the accumulation process. The configuration of the three array states were with one pinhole for the first array, two pinholes for the second state and three pinholes for the third state.

The 1D design of the array states were simulated according to the mentioned above conditions. In those simulations, the considerations of the design were to prevent zero points in the spectral filters' sum G(μ) and that the value of the filters' sum G(μ) transmission will be higher than the reference filter value in the region of interest (Figure 3). Note that in 1D design that were used although that there were two narrow spectral bands with the sum G(μ) lower in respect to the single pinhole system, the spectral information was preserved but with higher noise. However, the overall outcome of the time multiplexed array was still better than the results of single pinhole system. We note the P.T.F. x 1 time unit as P.T.F.T.-the Pinholes' Transfer Function computed in relative units. The transmission of one pinhole multiplied by the scan time of one image of time interval from the set of L, equal to one unit of P.T.F.T. The total accumulation time/L, equal to one time unit.

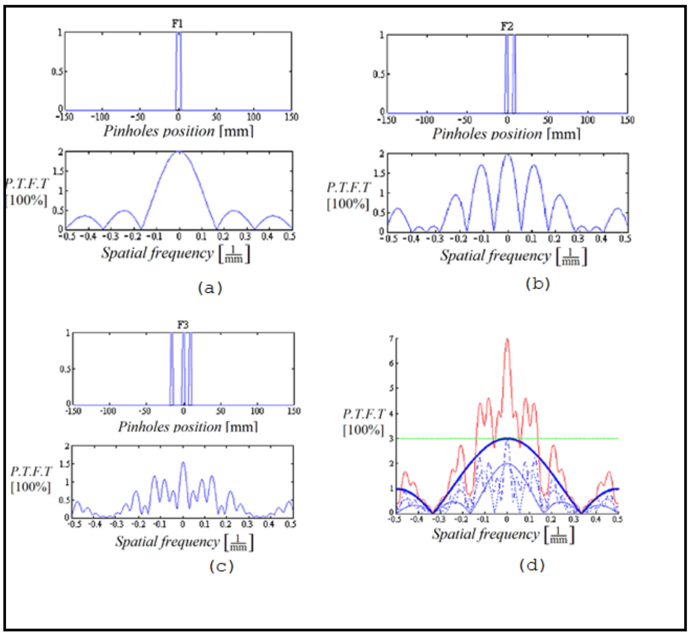

Figure 3) *Simulation of the 1D time multiplexed design (space domain and frequency domain): (a). The filter F1 related to the first array state; (b). The filter F2 related to the second array state; (c). The filter F3 related to the last array state; (d). The overall filter - sum of F1, F2, F3 (red) as compared to a single pinhole (coarse line blue). The straight green line is the reference level (maximum level of single pinhole).*

Experiment Results. In the next experiments the SPECT system was the GE Discovery NM/CT 670. The characteristics of the nuclear gamma detector were: 3/8" (9.5 mm) crystal thickness: 59 circular PMT's-53 × 3" (76 mm) and 6 × 1.5" (38 mm); Intrinsic spatial resolution: 3.6 mm; Usable field of view (UFOV): 54 × 40 cm ± 0.5 cm. The arrays (three array states) were made of lead with tungsten pinhole inserts. The pinhole insert diameter (δ): 4.45 mm; the distances of the setup were of magnification of 1: The distance between the object to the array (U): 14 cm; the distance between the array to the gamma detector distance (V): 14 cm; acceptance angle was: 750. The gamma radiation experimental validations were performed in the laboratories of General Electric Healthcare, Haifa, Israel and in the Nuclear Medicine unit at Shaare Zedek Medical Center, Jerusalem, Israel. The gamma system was configured and controlled according to the simulations parameters with super position of single pinhole. The object was a lead bar phantom (Figure 4). The results of the gamma system with bar phantom as an object are shown in Figure 5. The results showed the improvements of the 1D time multiplexed multi-pinhole array system (with 1D configuration mentioned above), compared with the reference single pinhole system. We achieved sensitivity efficiency improvement factor of 2.333 and SNR improvement factor of. The resolution (the same pinholes diameter) and scan time of both systems was the same. The next experiment was performed to emphasize the improvement of the proposed time multiplexed multi-pinhole system. With the single pinhole system an object (coin) was imaged in with short accumulation time (18 sec). The object was not recognized with 18 sec scan time in the captured image. Then, the same object was imaged with the time multiplexed multi-pinhole system with the same accumulation time (18 sec). Now, the object was well recognized as the result of the same object imaged with the single pinhole system after long accumulation time (42 sec).

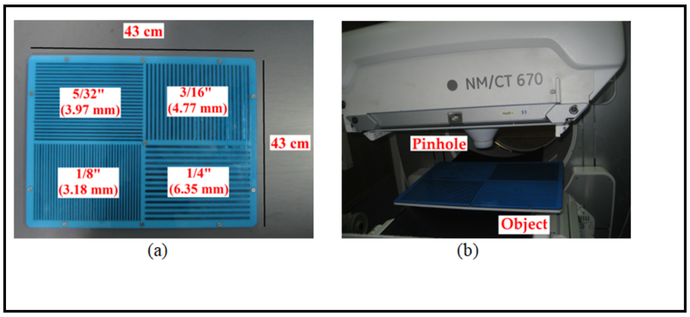

Figure 4 a) *The overall size of the bar phantom object (made of lead): 16-7/8" × 16-7/8" (43 × 43 cm), with the bar widths of: 1/4", 1/8", 3/16" and 5/32" (6.35, 3.18, 4.77, 3.97 mm);* b) *The bar phantom plate object in the radiation nuclear imaging NM/CT 670 SPECT system*

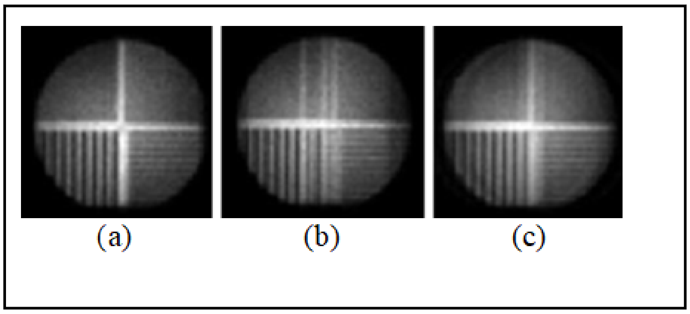

Figure 5) *The results of the gamma radiation nuclear imaging system: (a) The reference image of the single pinhole system; (b) The captured image of the 1D time multiplexed multi-pinhole array system; (c) The reconstructed image of the 1D time multiplexed multi-pinhole array system with sensitivity efficiency improvement factor of 2.333 and better SNR*

Thus, using the proposed concept, the time scan improvement factor was of 2.333. In order to correct the dome effect of the detector a uniformity correction was performed. The experiment results are shown. The comparison of SNR between the systems are presented in Table 1 and (Figure 6).

	Single pinhole system (avg. counts) accumulation time: 42 sec		**Multi-pinhole system (avg. counts) accumulation time: 18sec**	
	Signal	Noise (Std)	Signal	Noise (Std)
Object	4.061305	0.313631	4.242393	0.222412
Background	4.475837	0.2993	4.564631	0.26209

TABLE 1
The experiment SNR calculated results: The comparison of the imaged coin in the two systems.

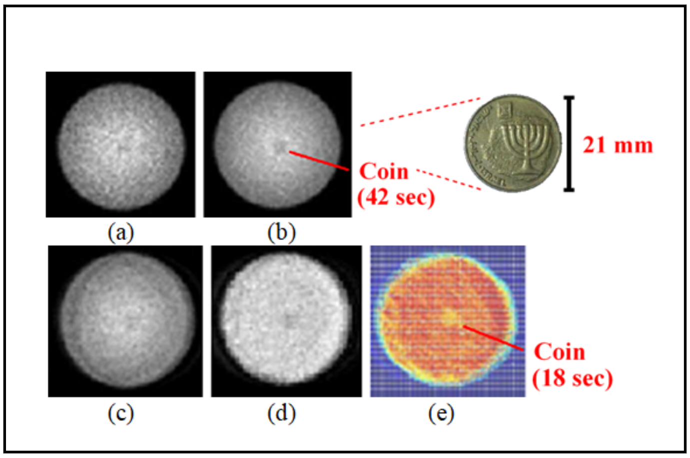

Figure 6) *Results of the coin object experiments (comparing scan time): (a) The single pinhole system image obtained after short scan time (18 sec)-the coin was not recognized; (b) The single pinhole system image obtained after long scan time (42 sec)-the coin was recognized; (c) The time multiplexed multi-pinhole array system image after short scan time (18 sec)-the captured image before reconstruction; (d) Reconstructed image-the coin was recognized after short scan time (18 sec); (e) Reconstructed image after dome effect correction*

By achieving those improvements, it enables to short the scan time by the factor correlated to the parameters of the time multiplexed multi-pinhole array system. Since the resolution of the system is related to the pinhole diameter, we compared the performance based on different pinholes size: Using 2 mm pinhole diameter for higher resolution (but with low counting rate and lower sensitivity) and 4.45 mm pinhole diameter for lower resolution (but with high counting rate and higher sensitivity). The single pinhole system was compared with the time multiplexed multi-pinhole array system using 2 mm pinholes (higher resolution) but now with higher sensitivity due to the high number of pinholes in the array). In the next experiment to show the resolution improvement of the time multiplexed multi-pinhole array system (with the same gamma radiation activity and scan time as compared to the single pinhole system), we used the follow ratio:

$$\frac{\pi R_1^2}{\pi R_2^2} = \frac{4.45^2}{2^2} = 4.95 \qquad (14)$$

The object was the bar phantom plate. The pinhole of the single pinhole system was with pinhole insert diameter (δ) of 4.45 mm while the pinholes of time multiplexed multi-pinhole array system were with pinhole insert diameter (δ) of 2 mm. The two pinhole inserts are shown in Figure 7. The improvement factor of the time multiplexed multi-pinhole array with 1D array design compared to the single pinhole system using 2 mm pinhole diameter in both systems is the total number of seven pinholes/three array states=2.333. The ratio of gamma radiation activity comparing two single pinhole systems, one of 2 mm pinhole diameter, and the second of 4.45 mm pinhole diameter is according to the ratio of the pinholes area (Eq. 14). By using a 2D design based on the same 1D design mentioned above, will give improvement factor of 5.667. The results of the resolution improvement of the time multiplexed multi-pinhole array system are shown in Figure 8.

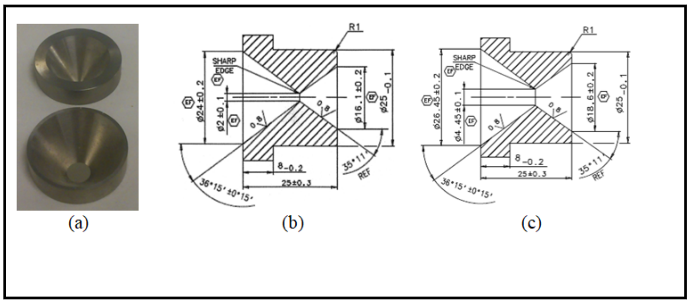

Figure 7a) *The two types of pinhole inserts made of tungsten: 2 mm (top) and 4.45 mm (bottom);* b) *The design of the 2 mm pinhole insert;* c) *The design of the 4.45 mm pinhole insert*

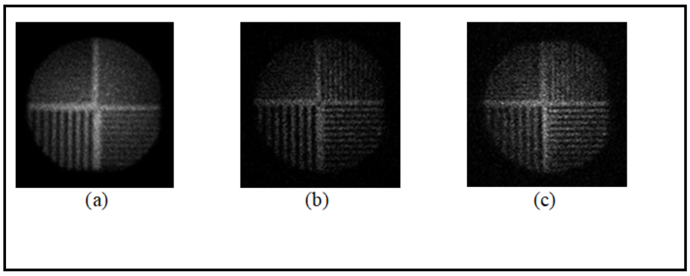

Figure 8) *Comparison of the systems with the same scan time (Sensitivity efficiency and SNR):* a) *The single pinhole system of 4.45 mm pinhole diameter with low resolution;* b) *The single pinhole system of 2 mm pinhole diameter with low sensitivity efficiency;* c) *Time multiplexed multi-pinhole array system of 2 mm pinholes diameter with high resolution and sensitivity efficiency*

CONCLUSION

In this paper, the first step towards developing a variable multiple pinhole nuclear imaging for gamma and x-rays systems was presented with the ability to obtain high resolution and high sensitivity for accurate tumors margin detection using targeted Nano-particles. This was accomplished by using known designs of multiple pinhole array coded aperture. We demonstrated that the desirable improvement can be achieved without changing the image resolution and without increasing the image acquisition time. The proposed concept was validated numerically and experimentally. The system can obtain depth information and 3D images using VCA system. The main challenge is the design considerations and the influence of the various parameters on the obtainable results. The experiments showed the system advantages: Short data acquisition time, reducing radioactive doses and radiation, high resolution images, improved SNR, simplicity and low cost. The method can be applied for near and far field systems and for many applications achieving the advantages that pinholes optics can offer.

REFERENCES

1. Rhyner MN, Smith AM, Yang L, et al. Quantum dots and multifunctional nanoparticles: New contrast agents for tumor imaging. Nanomed. 2006;1:1-9.
2. Kircher MF, de la Zerda A, Jokerst JV, et al. A brain tumor molecular imaging strategy using a new triple-modality MRI-photoacoustic-Raman nanoparticle. Nat Med. 2012;18:829-834.
3. Lin XZ, Wu ZY, Tao R, et al. Dual energy spectral CT imaging of insulinoma-Value in preoperative diagnosis compared with conventional multi-detector CT. Eur J Radiol. 2012;81:2487-2494.
4. Van Dam G.M, Themelis G, Crane LM, et al. Intraoperative tumor-specific fluorescence imaging in ovarian cancer by folate receptor-α targeting: First in-human results. Nat Med. 2011;17:1315-1319.
5. Gerard I J, Kersten-Oertel M, Petrecca K, et al. Brain shift in neuronavigation of brain tumors: A review. Med Image Anal. 2017;35:403-420.
6. Mansfield JR, Gossage KW, Hoyt CC, et al. Autofluorescence removal, multiplexing, and automated analysis methods for in vivo fluorescence imaging. J Biomed Opt. 2014;10:41-47.
7. Hoebe RA, Van Oven CH, Gadella TWJ, et al. Controlled light-exposure microscopy reduces photobleaching and phototoxicity in fluorescence live-cell imaging. Nat Biotechnol. 2007;25:249-253.
8. Carpentier P, Violot S, Blanchoin L, et al. Structural basis for the phototoxicity of the fluorescent protein KillerRed. FEBS Lett. 2009;583:2839-2842.
9. Ilovitsh T, Danan Y, Meir R, et al. Cellular imaging using temporally flickering nanoparticles. Sci Rep. 2015;5:82-84.
10. Ilovitsh T, Danan Y, Meir R, et al. Cellular superresolved imaging of multiple markers using temporally flickering nanoparticles. Sci Rep. 2015; 5:109-65.
11. Truong PL, Kim BW, Sim SJ, et al. Rational aspect ratio and suitable antibody coverage of gold nanorod for ultra-sensitive detection of a cancer biomarker. Lab Chip. 2012;12:1102-1109.
12. Zhan Q, Qian J, Li X, et al. A study of mesoporous silica-encapsulated gold nanorods as enhanced light scattering probes for cancer cell imaging. Nanotech. 2010;21:055-704.
13. Ankri R, Meiri A, Lau SI, et al. Intercoupling surface plasmon resonance and diffusion reflection measurements for real-time cancer detection. J Biophot. 2013;6:188-196.
14. Jaszczak RJ, Li J, Wang H, et al. Pinhole collimation for ultra-high-resolution, small-field-of-view SPECT. Phys Med Boil. 1994;39:425-437.
15. Hudson H, Larkin R. Accelerated image reconstruction using ordered subsets of projection data. IEEE Trans Med Image. 1994;13:601-609.
16. Vogel RA, Kirch D, Lefree M, et al. A New Method of multiplanar emission tomography using a seven pinhole collimator and an Auger Scintillation Camera. J Nucl Med. 1978;19:648-654.
17. LeFree MT, Vogel RA, Kirch DL, et al. Seven-pinhole tomography-A technical description. J Nucl Med. 1981;22:48-54.
18. Ivanovic M, Weber D, Loncaric S, et al. Multi-pinhole collimator optimization for high resolution SPECT imaging. IEEE Nuclear Sci Symp Conf Record. 2002;2:1097-1101.
19. Rowe RK, Aarsvold JN, Barrett HH, et al. A stationary hemispherical SPECT imager for three-dimensional brain imaging. J Nucl Med. 1993;34:474-480.
20. Klein W, Barrett H, Pang I, et al. Electrical and mechanical design of a high-resolution dynamic SPECT imager. IEEE Nucl Sci Symp Med Imag Conf Rec. 2002;2:931-933.
21. Furenlid LR, Wilson DW, Chen YC, et al. FastSPECT II: A Second-Generation High-Resolution Dynamic SPECT Imager. IEEE Trans Nucl Sci. 2004;51:631-635.
22. Beekman FJ, Vastenhouw B. Design and simulation of U-SPECT, an ultra-high resolution molecular imaging system. IEEE Nucl Sci Symp Med Imag Conf Record. 2004;2:792-796.
23. Meikle SR, Kench PL, Weisenberger A, et al. A prototype coded aperture detector for small animal SPECT. IEEE Trans Nucl Sci. 2002; 49:2167-2171.
24. Meikle SR, Wojcik R, Weisenberger AG, et al. CoALA-SPECT: A coded aperture laboratory animal SPECT system for pre-clinical imaging. IEEE Nucl Sci Symp Med Imag Conf Record. 2004;2:1061-1065.
25. Wilson DW, Barrett HH, Furenlid LR, et al. A new design for a SPECT small-animal imager. IEEE Nucl Sci Symp Conf Rec. 2002; 3:1826-1829.
26. Wilson D, Barrett H, Clarkson E. et al. Reconstruction of two- and three-dimensional images from synthetic-collimator data. IEEE Trans Med Imag. 2000; 19:412-422.
27. Beekman F, Van Der Have F, Vastenhouw B. et al. U-SPECT-I: A novel system for submillimeter-resolution tomography with radiolabeled molecules in mice. J Nucl Med. 2005; 46:1194-1200.
28. Van Der Have F, Vastenhouw B, Ramakers RM. et al. U-SPECT-II: An ultra-high-resolution device for molecular small-animal Imaging. J Nucl Med. 2009; 50:599-605.
29. McElroy D, Macdonald L, Beekman F, et al. Performance evaluation of A-SPECT: A high resolution desktop pinhole SPECT system for imaging small animals. IEEE Trans Nucl Sci. 2002; 49: 2139-2147.
30. Lackas C, Schramm N, Hoppin J et al. T-SPECT: A novel imaging technique for small animal research. IEEE Trans Nucl Sci. 2005; 52:181-187.
31. Ishizu K, Mukai T, Yonekura Y, et al. Ultra-high resolution SPECT system using four pinhole collimators for small animal studies. J Nucl Med. 1995;36(12):2282-7.
32. Wu MC, Hasegawa BH, Dae MW. Performance evaluation of a pinhole SPECT system for myocardial perfusion imaging of mice. Med Phys. 2002;29(12):2830-9.
33. Schramm NU, Ebel G, Engeland U, et al. High-resolution SPECT using multipinhole collimation. IEEE Trans Nucl Sci. 2003;50(3): 315-20.
34. Goertzen AL, Jones DW, Seidel J, et al. First results from the high-resolution mouseSPECT annular scintillation camera. IEEE Trans Med Imag. 2005;24(7):863-7.
35. Funk T, Després P, Barber WC, et al. A multipinhole small animal SPECT system with submillimeter spatial resolution. Med Phys. 2006;33(5):1259-68.
36. DiFilippo FP. Design and performance of a multi-pinhole collimation device for small animal imaging with clinical SPECT and SPECT–CT scanners. Phys Med Biol. 2008;53(15):4185.

37. Miller BW, Furenlid LR, Moore SK, et al. System integration of FastSPECT III, a dedicated SPECT rodent-brain imager based on BazookaSPECT detector technology. In2009 IEEE Nucl Sci Symp Confer Rec. 2009;4004-4008.
38. Peterson TE, Shokouhi S, Furenlid LR, et al. Multi-pinhole SPECT imaging with silicon strip detectors. IEEE Transac Nucl Sci. 2009;56(3):646-52.
39. Shokouhi S, Metzler SD, Wilson DW, et al. Multi-pinhole collimator design for small-object imaging with silispect: A high-resolution spect. Phys Medi Biol. 2008;54(2):207.
40. Vanhove C, Defrise M, Lahoutte T, et al. Three-pinhole collimator to improve axial spatial resolution and sensitivity in pinhole spect. Eur J Nucl Med Mol Imaging. 2008;35(2):407-15.
41. Branderhorst W, Vastenhouw B, Van Der Have F, et al. Targeted multi-pinhole spect. Eur J Nucl Med Mol Imaging. 2011;38(3):552-61.
42. Mertz L, Young NO. Fresnel transformations of images. SPIE milestone series ms. 1996;128:44-9.
43. Barrett HH, Wilson DT, DeMeester GD. The use of half-tone screens in Fresnel zone plate imaging of incoherent sources. Opt Commun. 1972;5(5):398-401.
44. Barrett HH, Horrigan FA. Fresnel zone plate imaging of gamma rays; theory. Appl Opt. 1973;12(11):2686-702.
45. Dicke RH. Scatter-hole cameras for x-rays and gamma rays. Astrophys J. 1968;153:L101.
46. Skinner GK. Imaging with coded-aperture masks. Nucl Instru Met Phys Res. 1984;221(1):33-40.
47. Stroke GW, Hayat GS, Hoover RB, et al. X-ray imaging with multiple-pinhole cameras using a posteriori holographic image synthesis. Opt Commun. 1969;1(3):138-40.
48. Chou C, Barrett HH. Gamma-ray imaging in Fourier space. Opt Lett. 1978;3(5):187-9.
49. Rosenfeld D, Macovski A. Time modulated apertures for tomography in nuclear medicine. IEEE Transac Nucl Sci. 1977;24(1):570-6.
50. Ohyama N, Honda T, Tsujiuchi J. Tomogram reconstruction using advanced coded aperture imaging. Opt Commun. 1981;36(6):434-8.
51. Ohyama N, Honda T, Tsujiuchi J, et al. Advanced coded-aperture imaging system for nuclear medicine. Appl Opt. 1983;22(22):3555-61.
52. Chi W, George N. Phase-coded aperture for optical imaging. Opt Commun. 2009;282(11):2110-7.
53. Chang LT, Macdonald B, Perez-Mendez V, et al. Coded aperture imaging of gamma-rays using multiple pinhole arrays and multiwire proportional chamber detector. IEEE Transac Nucl Sci. 1975;22(1): 374-8.
54. Cherry SR, Sorenson JA, Phelps ME. Physics in nuclear medicine e-Book. Elsev Heal Sci. 2012.
55. Fenimore EE. Coded aperture imaging: Predicted performance of uniformly redundant arrays. Appl Opt 1978;17(22):3562-70.
56. Accorsi R, Lanza RC. Near-field artifact reduction in planar coded aperture imaging. Appl Opt. 2001;40(26):4697-705.
57. Accorsi R, Gasparini F, Lanza RC. Optimal coded aperture patterns for improved SNR in nuclear medicine imaging. Nucl Instruments Methods Phys Res Sect A Accel Spectrom Detect Assoc Equip. 2001;474(3):273-84.
58. Accorsi R, Gasparini F, Lanza RC. A coded aperture for high-resolution nuclear medicine planar imaging with a conventional Anger camera: Experimental results. IEEE Transac Nuc Sci. 2001;48(6):2411-7.
59. Schwarz A, Shemer A, Zalevsky Z. Light intensity and SNR improvement for high-resolution optical imaging via time multiplexed pinhole arrays. Appl Opt. 2014;53(20):4483-92.
60. Schwarz A, Wang J, Shemer A, et al. Lensless three-dimensional integral imaging using variable and time multiplexed pinhole array. Opt Let. 2015;40(8):1814-7.
61. Tarantola A. Inverse problem theory and methods for model parameter estimation. Soc Indus Appl Math. 2005.
62. Thiébaut E. Introduction toimage reconstruction and inverse problems. Opt Astrophys. 2006;397-422.
63. Daube-Witherspoon ME, Muehllehner GE. An iterative image space reconstruction algorthm suitable for volume ECT. IEEE Trans Med Imaging. 1986;5(2):61-6.
64. Lantéri H, Soummer R, Aime C. Comparison between ISRA and RLA algorithms. Use of a Wiener Filter based stopping criterion. Astronom Astrophys Suppl Seri. 1999;140(2):235-46.